

Ultrahigh Critical Current Density across Sliding Electrical Contacts in Structural Superlubric State

Tielin Wu^{1,2}, Weipeng Chen^{1,2}, Lingyi Wangye^{1,2}, Yiran Wang^{1,3},
Zhanghui Wu^{1,2,*}, Ming Ma^{1,3,4,5,†} and Quanshui Zheng^{1,2,4,5,6,‡}

¹Center for Nano and Micro Mechanics, Tsinghua University, Beijing 100084, China


²Department of Engineering Mechanics, School of Aerospace Engineering, Tsinghua University, Beijing 100084, China

³Department of Mechanical Engineering, Tsinghua University, Beijing 100084, China

⁴State Key Lab of Tribology in Advanced Equipment (SKLT), Tsinghua University, Beijing 100084, China

⁵Institute of Superlubricity Technology, Research Institute of Tsinghua University in Shenzhen, Shenzhen 518057, China

⁶Tsinghua Shenzhen International Graduate School, Shenzhen 518057, China

 (Received 16 June 2023; revised 1 December 2023; accepted 6 February 2024; published 1 March 2024)

In conventional sliding electrical contacts (SECs), large critical current density (CCD) requires a high ratio between actual and apparent contact area, while low friction and wear require the opposites. Structural superlubricity (SSL) has the characteristics of zero wear, near zero friction, and all-atoms in real contact between the contacting surfaces. Here, we show a measured current density up to 17.5 GA/m² between microscale graphite contact surfaces while sliding under ambient conditions. This value is nearly 146 times higher than the maximum CCD of other SECs reported in literatures (0.12 GA/m²). Meanwhile, the coefficient of friction for the graphite contact is less than 0.01 and the sliding interface is wear-free according to the Raman characterization, indicating the presence of the SSL state. Furthermore, we estimate the intrinsic CCD of single crystalline graphite to be 6.69 GA/m² by measuring the scaling relation of CCD. Theoretical analysis reveals that the CCD is limited by thermal effect due to the Joule heat. Our results show the great potential of the SSL contacts to be used as SECs, such as micro- or nanocontact switches, conductive slip rings, or pantographs.

DOI: 10.1103/PhysRevLett.132.096201

Introduction.—Sliding electrical contacts (SECs) are widely used in many devices to transmit current or signals, such as micromotors [1], switches, relays [2–4], accelerometers [5], and storage in microelectromechanical systems [6]. On a larger scale, the performance of conductive slip rings [7] and pantographs [8] is also determined by SECs. The critical current density (CCD) of SECs is the maximum current that can maintain the normal operation of the SEC under operation conditions. In the literature, CCD for friction pairs is characterized in three ways. The first is where significant wear starts [9–12], the second marks the onset of material melting [13,14], and the third—used here—indicates when interface defects emerge, presenting the strictest measure. High CCD in SECs enhances power transmission and enables device miniaturization.

SECs depend on low contact resistance for efficient energy transfer and minimal loss [12,15]. High resistance engenders Joule heating at interfaces, precipitating energy loss and failure [15–17]. Thus, ensuring a low contact resistance at the interface is crucial for achieving high-energy density transmission while mitigating heat-related interface failures. Commonly employed strategies involve the implementation of noble metals such as copper, silver, platinum, and gold as coating layers between sliding interfaces to reduce contact resistance [15,16,18].

Utilization of noble metals to diminish contact resistance paradoxically augments friction and wear, thereby reducing device longevity [12], and the resultant debris risks electrical shorts [19]. Research into two-dimensional materials like graphene aims to mitigate these issues, though they may raise interface resistance [20,21]. Strategies modifying graphite-to-copper ratios have seen some success in simultaneously lowering friction and resistance; nevertheless, the outcomes indicate persistently high interface resistivity (4000 Ω μ m) and friction coefficients (0.255) [22].

Structural superlubricity (SSL) is a state of zero wear and ultralow friction between two contact solid surfaces [23], which would bring disruptive changes to SECs. SSL has been achieved between graphite and a wide range of other materials (such as MoS₂, DLC, Au, etc. [23]) with air-craft speed (294 m/s) at the graphite-graphite interface [24]. In addition, experiments have shown that the SSL state can persist with a sliding distance up to 100 km [25]. Considering that the actual contact area of the SSL system is approximately equal to the apparent contact area (details in Discussion) [25,26] and the excellent thermal stability of graphite [27,28], it is expected that SSL graphite contact is a good candidate to resolve the contraction between high CCD, and low friction as well as wear for conventional SECs. Yet, no relevant studies have been reported.

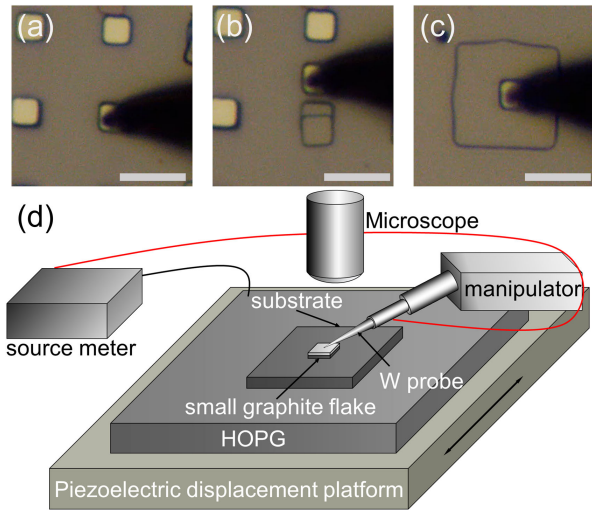


FIG. 1. Experimental setup. (a)–(c) The process of transferring graphite flake. We shear the Pt-cap graphite mesa with tungsten probe precisely controlled by a micromanipulator. The $4\ \mu\text{m} \times 4\ \mu\text{m}$ flake is stuck to the tip of probe and placed on the surface of a freshly cleaved $14\ \mu\text{m} \times 14\ \mu\text{m}$ substrate. Scale bar, $10\ \mu\text{m}$. (d) The illustration of our experimental setup.

In this Letter, SSL with ultrahigh CCD of $17.5\ \text{GA}/\text{m}^2$ is realized for the first time under ambient conditions. Such a high value is 146 times larger than the existing CCD of SECs reported in the literature ($0.12\ \text{GA}/\text{m}^2$ for Au/Cu friction pair [29]). Typical characteristics of SSL, i.e., low coefficient of friction (<0.01) and negligible wear, is observed. According to the theoretical and experimental results, it is found that CCD converges to $6.69\ \text{GA}/\text{m}^2$ with the increase of flake size.

Main.—Our experimental samples are graphite mesas, as shown in Fig. 1(a), fabricated by electron beam lithography process on a freshly cleaved highly oriented pyrolytic graphite (HOPG, Bruker, ZYB grade). Detailed preparation process can be found in Sec. 1 in the Supplemental Material [30]. A $200\ \text{nm}$ thick Pt cap is deposited on the $1\ \mu\text{m}$ height graphite mesa as a conductive connection. We use a micromanipulator MM3A (Kleindiek) controlling a tungsten probe with a tip radius of 1 to $2\ \mu\text{m}$ to transfer the graphite flakes to fabricate a graphite-graphite homojunction. The fabricated homojunction is composed of a small graphite flake ($4\ \mu\text{m} \times 4\ \mu\text{m}$) on a freshly sheared graphite surface serving as substrate, as illustrated in Figs. 1(a)–1(c). We choose the graphite flakes with a single crystalline surface on the bottom through the self-retraction motion [39] (detailed in Sec. 2 of the Supplemental Material [30]).

A homemade system is built to measure the current transferred by the fabricated graphite homojunctions as shown in Fig. 1(d). HOPG with graphite substrate covered by small graphite flake is fixed on the top of piezoelectric displacement platform (XMT, E01.D3), while the tungsten

probe is pressed on the small graphite flake covered by a Pt cap. Periodic reciprocating motion between graphite homojunctions is performed by driving the piezoelectric displacement platform with an amplitude of $1\ \mu\text{m}$ and frequency of $3\ \text{Hz}$, while the tungsten probe remains still. By applying a voltage bias V_b between the HOPG substrate and the tungsten probe through a source meter (Keithley 2450) while measuring the current simultaneously, we can obtain the current transferred by the graphite homojunctions. All the experiments are performed under ambient environment (temperature: $20\text{--}25\ ^\circ\text{C}$, relative humidity: $20\%\text{--}30\%$).

Then, we measure the CCD, which is the maximum current density to maintain SSL between graphite flake and substrate, for individual graphite homojunctions as shown in Fig. 1(d). With each current measured, the current density J can be calculated by dividing the current by the contact area between graphite flake and graphite substrate, which is typically $3\ \mu\text{m} \times 3\ \mu\text{m}$. With each current density ($J = 10.56, 15.56, 16.67,$ and $17.78\ \text{GA}/\text{m}^2$), we apply the current for a duration of $2.4\ \text{sec}$. Such duration is larger than the time required by the graphite homojunction to reach steady state, t_{st} . The value of t_{st} is estimated to be about $10^{-6}\ \text{sec}$ by finite element simulation, as shown in Sec. 3 of the Supplemental Material [30]. By increasing J from 10.56 to $17.78\ \text{GA}/\text{m}^2$, and characterizing the sliding surface of graphite substrate after each current density using Raman spectroscopy, we find that the defects only occur when J is larger than $10.56\ \text{GA}/\text{m}^2$, as indicated by the presence of the D peak in Figs. 2(a) and 2(b), which corresponds to a defect density of $185.2/\mu\text{m}^2$ [40–42].

Furthermore, we measure the dependence of friction force on normal load for the graphite homojunction. Specifically, for J being $0, 16.67,$ and $17.78\ \text{GA}/\text{m}^2$, we measure the friction force both for loading and unloading processes, as shown in Fig. 2(c). For $J = 0$ and $16.67\ \text{GA}/\text{m}^2$, the dependence of friction on normal force remains the same in both loading and unloading processes, and the differential coefficient of friction (dCOF) is 0.00141 and 0.00135 , respectively. For $J = 17.78\ \text{GA}/\text{m}^2$, however, the friction doubles to nearly $1\ \mu\text{N}$ compared to before, and the dCOF increases to 0.00546 for loading and 0.00925 for unloading. This significant rise in friction and the disparity in loading and unloading curves suggests wear at the interface. This set of measurements show that the critical current density J_c of the SSL interfaces is between 16.67 and $17.78\ \text{GA}/\text{m}^2$, which is nearly 139 times the maximum current density ($0.12\ \text{GA}/\text{m}^2$ for Au/Cu friction pair) reported in the literature [29]. Similar measurement presents that SSL is also observed with larger normal force as shown in Sec. 4 in the Supplemental Material [30], which shows the coefficient of friction being 0.006 .

For an ideal graphite homojunction with a given size and operation condition, J_c should be an intrinsic property. However, as SSL graphite contact surfaces could contain

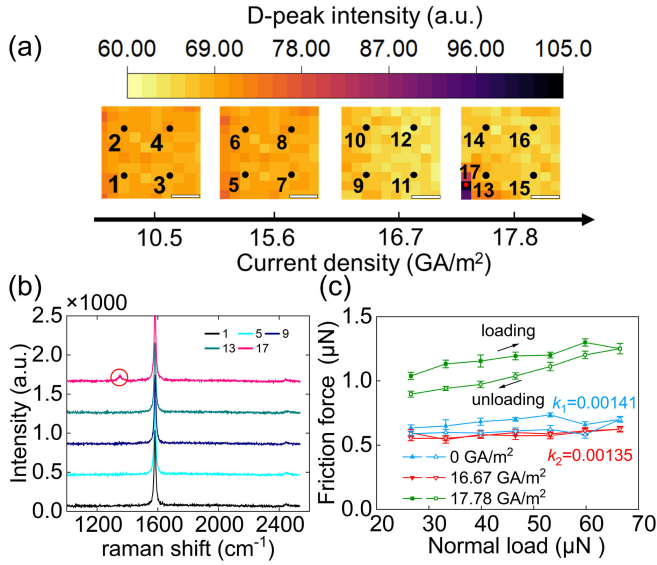


FIG. 2. The measurements of CCD between graphite interfaces. (a) Raman spectroscopy mappings of the graphite substrate's sliding surface after sliding with different current densities from small to large (10.5, 15.6, 16.7, and 17.8 GA/m²). We scanned the Raman spectroscopy mapping after each test. Scale bar, 2 μm. (b) Raman spectroscopy curves of different points marked in (a) with the Raman shift from 1000 to 2400 cm⁻¹. (lines 1 to 17 from bottom to top, marked with a red circle at peak D of line 17, The lines not shown are similar to lines 1, 5, 9, and 13). (c) The relationship between friction and normal load before (0 GA/m²) and after (16.7 and 17.8 GA/m²) different current densities.

internal steps or buried buckles [26] which could result in different CCD, there could be variation in the measured J_c . As defects would increase the electrical resistance of graphite [43], aiming at obtaining the intrinsic value of J_c , for a given size of graphite homojunction, we measure J_c for multiple samples under the same condition. Specifically, for each graphite homojunction sample, a series of current densities from low to high is applied via the output of the current source. After each electrical test, we characterize the defect of the sliding surfaces by Raman spectrum as explained before. The maximum current density without defect, i.e., J_c , is then obtained for the sample. For a set of samples with the same size, the maximum J_c is then chosen as the intrinsic value of J_c for graphite homojunction with a given side length, J_c^L , as shown in Fig. 3(a). In this case, there is no error bar for J_c^L . Furthermore, we also measure the intrinsic value of J_c for graphite homojunction with different side length L .

From Fig. 3(b), it is clear that J_c^L decreases with the increase of the size L , with the highest value of 17.5 GA/m² at $L = 2$ μm. Such dependence can be quantitatively understood with the model proposed below. For a given graphite homojunction, the Joule heating power per unit contact area (P_0) can be written as

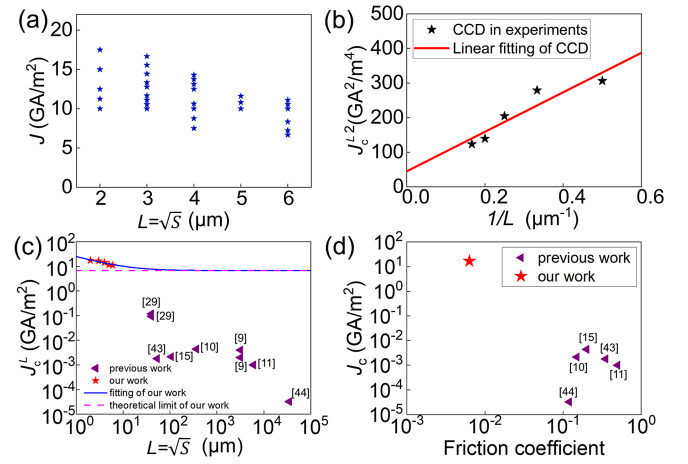


FIG. 3. The scaling relation of CCD and comparison with existing reports. (a) The relationship between CCD and sizes of graphite flakes. For each size, multiple samples are tested to obtain the intrinsic value of CCD. (b) The relationship between the square of CCD (J_c^L)² and the size of the graphite flake. (c) The relationship between CCD and the size of the contact. The red and purple points represent our and previous work [9–11,15,29,44,45], respectively. The blue line is the fitting according to Eq. (3). (d) The relationship between the CCD and the friction coefficient. The red and purple points represent our and previous work [10,11,15,44,45], respectively.

$$P_0 = \frac{P}{S} = \frac{I^2 R}{S} = \frac{I^2}{\sigma L^2}, \quad (1)$$

where P is the whole power of the interfaces due to Joule heating, S is the contact area, I is the current of the circuit, L is the length of small graphite flake, R and σ are the resistance and conductance of the sliding interface, respectively. For small graphite flake on a larger surface as studied here, the interface's conductance can be divided into two parts: edge to in-plane conductance density σ_{ed} and in-plane to in-plane conductance density σ_{in} [46]. Therefore, the sliding interface conductance is

$$\sigma = 4\sigma_{ed}\delta L + \sigma_{in}(L - 2\delta)^2, \quad (2)$$

where δ is the width of the flake's edge. Combining Eqs. (1) and (2), we can derive P_0 as

$$P_0(J, L) = \frac{J^2}{\frac{4(\sigma_{ed} - \sigma_{in})\delta}{L} + \sigma_{in}}, \quad (3)$$

where J is the current density of the SSL interface.

For our system, the generation of interfaces' defects is mainly caused by thermal excitation [27]. Using finite element analysis, we find that the heat dissipation power per unit area is almost the same for each (J_c^L, L) (details in Sec. 3 of the Supplemental Material [30]). Therefore, the Joule heating power per unit area introducing defects in graphite at different scales should be the same. Therefore,

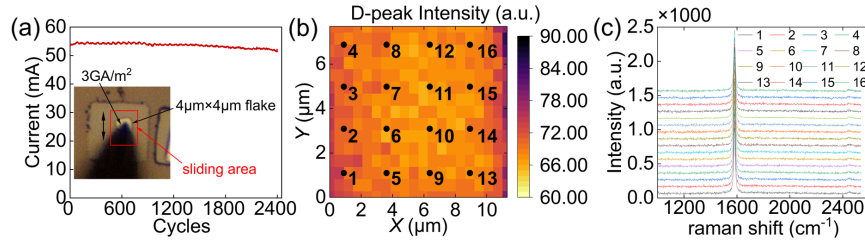


FIG. 4. The durability of SSL SEC carrying large current. (a) The transmitting current during more than 2000 cycles under the 0.5 V bias voltage. The amplitude and frequency of the cycle are 1 μm and 3 Hz. (b) Raman mapping of the sliding area. The brightness represents the signal intensity around the defecting peak ($\sim 1350\text{ cm}^{-1}$). (c) Raman signals of different points in (b) with the Raman shift from 1000 to 2400 cm^{-1} .

$P_0(J_c^L, L)$ should be constant. And because the prominent zero-energy edge states, typically localized at zigzag graphene terminations, are strongly involved in the transport process according to the literature results [46], σ_{ed} is greater than σ_{in} , which means the square of CCD (J_c^L)² should be proportional to $1/L$ according to Eq. (3). Indeed, this is what we observed in experiment as shown in Fig. 3(b). In addition, the frictional heating power is orders smaller than the Joule heating (see Sec. 5 in [30]). The normal load used in our experiments is much smaller than that required to induce defects directly which is about 1 GPa [47] and has negligible influence on contact resistance (see Sec. 6 in [30]). Thus, we believe that the Joule heating power per unit area is the main cause leading to the failure of the graphite-graphite sliding interface.

As an intrinsic property for SEC based on SSL graphite, it is important to estimate its value. To this end, we fit J_c^L versus L according to Eq. (3), and find that $J_c^\infty = 6.69\text{ GA/m}^2$. Such a high value (55 times larger than the reported value) indicates the potential of single crystalline graphite to be used as a macroscopic electrical contact. This is further supported by comparing our results with the existing CCD above which the SEC will either be worn out or eroded by current for different types of SEC in different sizes [Fig. 3(c)]. It is evident that our SSL graphite holds the largest CCD across all scales, being 2 orders larger at least. Besides J_c , the COF is another important property for SECs. Therefore, we plot J_c versus COF for existing reports together with our measurement as shown in Fig. 3(d). Obviously, our SSL graphite homojunction holds the lowest COF and highest J_c among all the SECs, both being orders smaller or larger than other SECs, demonstrate the superior properties to be used as an ideal SEC.

As an application, we slide the small graphite flake for more than 2000 cycles under a 0.5 V constant voltage, and record the current of the circuit at the same time, mimicking a minimum viable product for SEC. The sliding amplitude and frequency is 1 μm and 3 Hz, respectively. As shown in Fig. 4(a), the current density is stable across all the cycles, with a value about 3 GA/m^2 , which is 25 times higher than existing reported value 0.12 GA/m^2 [29]. Furthermore, we characterize the sliding interfaces by Raman spectroscopy

for detecting whether the defects occur at the sliding area, and the results are shown in Figs. 4(b) and 4(c). The uniform signal intensity of the D peak ($\sim 1350\text{ cm}^{-1}$) indicates the whole sliding area shares similar defect intensity if any [Fig. 4(b)]. Therefore, we select 16 positions of the sliding area and find that their defect densities are all below $80/\mu\text{m}^2$, indicating the absence of wear [40–42].

Discussion.—Our findings highlight the exceptional attributes of SSL graphite-based SEC, referred to as SSL SEC. The high CCD is primarily attributed to its superior conductivity and thermal stability, with the latter influenced by actual contact area and phonon-assisted transport mechanisms [48–50]. Traditional SECs like Au/Au [21], often feature uneven atomic-level contact areas, resulting in much smaller actual contact areas compared to apparent ones. In contrast, SSL SECs utilize a two-dimensional interface with atomically smooth, fully contacted surfaces (interface details in Sec. 7 of the Supplemental Material [30]) [25], providing a notable advantage in current transmission contact area. The full contact contributes to not only the electrical resistance reduction, but also the heat dissipation improvement, leading to the large CCD. Using the four-wire method, the graphite-graphite interface’s contact resistivity we measured is $9.34 \times 10^{-10}\ \Omega\ \text{m}^2$ (details in Sec. 8 of [30]), consistent with other measurement results $1.66 \times 10^{-10}\ \Omega\ \text{m}^2$ [46], 0.3×10^{-9} – $1.5 \times 10^{-9}\ \Omega\ \text{m}^2$ [51], and is 1/3 of the copper-graphite contact [52], a standard industrial SEC. Despite metals achieving atomic smoothness when polished, issues such as cold welding and high friction can impede their use in sliding pairs [53]. Therefore, the core advantage of the SSL SEC interface is its high actual contact area combined with an exceptionally low friction level, a crucial feature of its underlying SSL technology [23,54].

The SSL’s low friction and wear-free properties from its defect-free 2D structure, requiring thermal stability during conductive sliding. Joule heating from conduction could incite carbon atom movement in the graphene, risking structural integrity. However, graphene’s robust C-C bonds and high Young’s modulus stabilize the hexagonal structure in the SSL SEC, protecting the interface. [55,56]. Additionally, while covalent bonding between graphene layers could disrupt the structure during sliding, the bond

strength at the SSL SEC interface surpasses that of typical carbon films and metals, mitigating damage risks [57,58]. Additionally, graphene is well known for its excellent thermal stability. Monolayer graphene begins to exhibit defects at around 500 °C in air, while bilayer graphene exhibits this behavior at around 600 °C [27,28]. The thermal stability of graphene is positively correlated to its number of layers due to the interlayer interactions [27,28]. Therefore, we can infer that the graphite flake used here would have superior thermal stability. According to the finite element simulation in Fig. S2, the graphite interface temperature of steady state is about 946 °C which is consistent with the experimentally measured temperature at which defects start to appear in graphite [27,28]. Altogether, the synergistic effects of relative low contact resistivity, excellent tribological properties, and high thermal stability of SSL graphite homojunction make it an ideal candidate for a SEC, as demonstrated by our experiments. Moreover, investigating the origins and evolution patterns of in-plane defects at the interface remains a valuable endeavor. This can be explored by monitoring alterations in Raman spectroscopic mappings while applying currents beyond the CCD value and managing the sliding or stationary conditions.

Conclusion.—In summary, we find experimentally that the graphite-graphite interface is able to transmit ultrahigh current density (17.5 GA/m²), 2 orders larger than the reported value of other SECs. Such extraordinary property is contributed to the synergies of relative low contact resistivity, excellent tribological properties, and high thermal stability of SSL graphite homojunction. As a minimum viable product for SEC, we exhibited the durability of our graphite-graphite SEC with a wear-free sliding over 2000 cycles under high current densities (~3 GA/m²), showing its great potential in applications such as slip rings and micro- or nanoelectro-mechanical switches.

However, there remain various unresolved concerns pertaining to the robustness of SSL SEC. These include dependencies on factors like velocity, temperature, and atmospheric conditions. Furthermore, the feasibility of producing large-scale single-crystal graphite has been demonstrated [59], raising the challenging question of whether it is possible to achieve experimental realization of SSL SEC on a larger scale. Another valuable area of exploration is the extension of the 2D/2D homojunction contacts of SSL SEC to encompass 2D/3D heterojunction systems.

The authors wish to acknowledge the financial support by National Natural Science Foundation of China (Grants No. 11572173, No. 51961145304, No. 11921002, No. 11890671, No. 11890673, and No. 12204321), Ministry of Science and Technology of the People's Republic of China (No. 2023YFB4603601), China Postdoctoral Science Foundation (No. BX20220181), and the Shenzhen Fundamental Research Key Project (No. JCYJ20200109150608043). Shenzhen Science and Technology Program (JCYJ20210324100600001).

*Corresponding author: wuzh1995@mail.tsinghua.edu.cn

†Corresponding author: maming16@tsinghua.edu.cn

‡Corresponding author: zhengqs@tsinghua.edu.cn

- [1] T. Morita, *Sens. Actuators A* **103**, 291 (2003).
- [2] A. Basu, G. G. Adams, and N. E. McGruer, *J. Micromech. Microeng.* **26**, 104004 (2016).
- [3] O. Y. Loh and H. D. Espinosa, *Nat. Nanotechnol.* **7**, 283 (2012).
- [4] B. Ma, Z. You, Y. Ruan, S. Chang, and G. Zhang, *Microsyst. Technol.* **22**, 911 (2015).
- [5] S. Arjun, Y. Navid, and N. Khalil, *J. Micromech. Microeng.* **11**, 118 (2001).
- [6] B. Bhushan and K. J. Kwak, *Nanotechnology* **18**, 345504 (2007).
- [7] M. Grandin and U. Wiklund, in *ICEC 2014; The 27th International Conference on Electrical Contacts 2014* (IEEE, San Diego, 2014), p. 1.
- [8] J. Ambrósio, J. Pombo, M. Pereira, P. Antunes, and A. Mósca, *Int. J. Railw. Technol.* **1**, 249 (2012).
- [9] K. A. Aleutdinov, V. Y. Rubtsov, V. V. Fadin, and M. I. Aleutdinova, *IOP Conf. Ser.* **116**, 012022 (2016).
- [10] N. Argibay, J. A. Bares, J. H. Keith, G. R. Bourne, and W. G. Sawyer, *Wear* **268**, 1230 (2010).
- [11] Y. A. Wang, J. X. Li, Y. Yan, and L. J. Qiao, *Tribol. Int.* **50**, 26 (2012).
- [12] J. A. Bares, N. Argibay, N. Mauntler, G. J. Dudder, S. S. Perry, G. R. Bourne, and W. G. Sawyer, *Wear* **267**, 417 (2009).
- [13] P. G. Slade, *Electrical Contacts: Principles and Applications* (CRC Press, Boca Raton, 2017).
- [14] R. Holm, *Electric Contacts: Theory and Application* (Springer Science & Business Media, New York, 2013).
- [15] N. Argibay and W. G. Sawyer, *Wear* **274–275**, 229 (2012).
- [16] M. Grandin and U. Wiklund, *Tribol. Int.* **121**, 1 (2018).
- [17] A. Senouci, H. Zaidi, J. Frene, A. Bouchoucha, and D. Paulmier, *Appl. Surf. Sci.* **144–145**, 287 (1999).
- [18] C. Holzapfel, P. Heinbuch, and S. Holl, in *2010 Proceedings of the 56th IEEE Holm Conference on Electrical Contacts* (IEEE, Charleston, 2010), p. 1.
- [19] I. H. Sung, J. W. Kim, H. J. Noh, and H. Jang, *Tribol. Int.* **95**, 256 (2016).
- [20] B. H. Chudnovsky, in *Proceedings of the Fifty-First IEEE Holm Conference on Electrical Contacts* (IEEE, Chicago, 2005), p. 107.
- [21] M. Grandin and U. Wiklund, *Wear* **398–399**, 227 (2018).
- [22] K. H. Cho, U. S. Hong, K. S. Lee, and H. Jang, *Tribol. Lett.* **27**, 301 (2007).
- [23] O. Hod, E. Meyer, Q. Zheng, and M. Urbakh, *Nature (London)* **563**, 485 (2018).
- [24] D. Peng, Z. Wu, D. Shi, C. Qu, H. Jiang, Y. Song, M. Ma, G. Aeppli, M. Urbakh, and Q. Zheng, *Proc. Natl. Acad. Sci. U.S.A.* **117**, 12618 (2020).
- [25] D. Peng, J. Wang, H. Jiang, S. Zhao, Z. Wu, K. Tian, M. Ma, and Q. Zheng, *Natl. Sci. Rev.* **9**, nwab109 (2022).
- [26] K. Wang, C. Qu, J. Wang, B. Quan, and Q. Zheng, *Phys. Rev. Lett.* **125**, 026101 (2020).
- [27] F. Liu, M. Wang, Y. Chen, and J. Gao, *J. Solid State Chem.* **276**, 100 (2019).
- [28] H. Y. Nan, Z. H. Ni, J. Wang, Z. Zafar, Z. X. Shi, and Y. Y. Wang, *J. Raman Spectrosc.* **44**, 1018 (2013).

- [29] S. H. Fan and Y. C. Chan, *J. Electron. Mater.* **32**, 101 (2003).
- [30] See Supplemental Material at <http://link.aps.org/supplemental/10.1103/PhysRevLett.132.096201> for sample fabrication, self-retracting motion, finite element simulation, supplementary friction test, discussion on frictional heating and Joule's heating from transmission current, contact resistance and positive pressure correlation, high-resolution cross-sectional images of the graphite-graphite interface and four-probe method for measuring electrical properties of graphite contacts, which includes Refs. [31–38].
- [31] Q. Zheng, B. Jiang, S. Liu, Y. Weng, L. Lu, Q. Xue, J. Zhu, Q. Jiang, S. Wang, and L. Peng, *Phys. Rev. Lett.* **100**, 067205 (2008).
- [32] N. J. Luiggi and W. Barreto, *Phys. Rev. B* **34**, 2863 (1986).
- [33] A. Alofi and G. P. Srivastava, *Phys. Rev. B* **87**, 115421 (2013).
- [34] L. Zhong, L. Guo, J. Wang, Q. Song, H. Li, and Y. Li, *Carbon* **208**, 123 (2023).
- [35] M. Inagaki, Y. Kaburagi, and Y. Hishiyama, *Adv. Eng. Mater.* **16**, 494 (2014).
- [36] H. Zhang, X. Chen, Y.-D. Jho, and A. J. Minnich, *Nano Lett.* **16**, 1643 (2016).
- [37] E. Koren, A. W. Knoll, E. Lörtscher, and U. Duerig, *Nat. Commun.* **5** (2014).
- [38] S. Picard, D. T. Burns, and P. Roger, *Metrologia* **44**, 294 (2007).
- [39] Z. Liu, J. Yang, F. Grey, J. Z. Liu, Y. Liu, Y. Wang, Y. Yang, Y. Cheng, and Q. Zheng, *Phys. Rev. Lett.* **108**, 205503 (2012).
- [40] D. M. Basko, S. Piscanec, and A. C. Ferrari, *Phys. Rev. B* **80**, 165413 (2009).
- [41] L. G. Cançado, A. Jorio, E. H. Martins Ferreira, F. Stavale, C. A. Achete, R. B. Capaz, M. V. O. Moutinho, A. Lombardo, T. S. Kulmala, and A. C. Ferrari, *Nano Lett.* **11**, 3190 (2011).
- [42] A. C. Ferrari and D. M. Basko, *Nat. Nanotechnol.* **8**, 235 (2013).
- [43] A. Arndt, D. Spoddig, P. Esquinazi, J. Barzola-Quiquia, S. Dusari, and T. Butz, *Phys. Rev. B* **80**, 195402 (2009).
- [44] J. A. Bares, N. Argibay, N. Mauntler, G. J. Dudder, S. S. Perry, G. R. Bourne, and W. G. Sawyer, *Wear* **267**, 417 (2009).
- [45] Z. He, Z. Ni, H. Wang, Z. Yang, W. Wei, X. Wang, L. Deng, and G. Wu, in *2021 International Conference on Electrical Materials and Power Equipment (ICEMPE)* (IEEE, Chongqing, 2021), p. 1.
- [46] D. Dutta, A. Oz, O. Hod, and E. Koren, *Nat. Commun.* **11**, 4746 (2020).
- [47] T. Sun, Z. Wu, Z. Li, Q. Zheng, and L. Lin, *Sensors (Basel)* **19**, 3431 (2019).
- [48] V. Perebeinos, J. Tersoff, and P. Avouris, *Phys. Rev. Lett.* **109**, 236604 (2012).
- [49] E. Koren, I. Leven, E. Lortscher, A. Knoll, O. Hod, and U. Duerig, *Nat. Nanotechnol.* **11**, 752 (2016).
- [50] Y. Kim *et al.*, *Phys. Rev. Lett.* **110**, 096602 (2013).
- [51] M. R. Vazirisereshk, S. A. Sumaiya, A. Martini, and M. Z. Baykara, *Appl. Phys. Lett.* **115**, 091602 (2019).
- [52] B. D. Beake, A. J. Harris, T. W. Liskiewicz, J. Wagner, S. J. McMaster, S. R. Goodes, A. Neville, and L. Zhang, *Wear* **474–475**, 203866 (2021).
- [53] A. J. W. Moore, *Proc. R. Soc. A* **195**, 231 (1948).
- [54] M. Dienwiebel, G. S. Verhoeven, N. Pradeep, J. W. M. Frenken, J. A. Heimberg, and H. W. Zandbergen, *Phys. Rev. Lett.* **92**, 126101 (2004).
- [55] H. I. Rasool, C. Ophus, W. S. Klug, A. Zettl, and J. K. Gimzewski, *Nat. Commun.* **4**, 2811 (2013).
- [56] C. Lee, X. Wei, J. W. Kysar, and J. Hone, *Science* **321**, 385 (2008).
- [57] P. L. de Andres, R. Ramírez, and J. A. Vergés, *Phys. Rev. B* **77**, 045403 (2008).
- [58] J. Sun, Y. Zhang, Z. Lu, Q. Li, Q. Xue, S. Du, J. Pu, and L. Wang, *J. Phys. Chem. Lett.* **9**, 2554 (2018).
- [59] C. Liu and K. Liu, *Nat. Nanotechnol.* **17**, 439 (2022).